Appl. Phys. B 86, 721–727 (2007)
DOI: 10.1007/s00340-006-2542-1

Applied Physics B
Lasers and Optics

A.J. MOULÉ
K. MEERHOLZ✉

Minimizing optical losses in bulk heterojunction polymer solar cells

Institut für Physikalische Chemie, Universität zu Köln, Luxemburgerstr. 116, 50939 Köln, Germany

Received: 20 July 2006/Revised version: 7 November 2006
Published online: 22 December 2006 • **© Springer-Verlag 2006**

ABSTRACT The efficiency that a solar cell can reach is ultimately limited by the number of photons absorbed in its active layer. Bulk heterojunction polymer solar cells are fabricated from a stack of thin film layers, each of which is thinner than a single wavelength from an incident photon within its absorption band. One consequence of this thin film layer stack is a strong optical interference between the various layers that can change the quantity of light dissipated in the active layer by 50%. Here we use optical modeling to quantitatively calculate the dissipation in each of the various layers as functions of wavelength and layer thickness. Using this information the loss free short circuit current density can be calculated (J_{sc}max). Optimization of J_{sc}max leads to direct improvements in the efficiency of the solar cell through improved light dissipation in the active layer. The optical properties for a P3HT:PCBM active layer and a model Lorentzian low band gap spectrum are optimized and ideal fabrication conditions are reported for these materials.

PACS 72.40.+w; 72.80.Le

1 Introduction

Over recent years polymer photovoltaics have been studied because they have the potential to be low cost, solution processable, and compatible with flexible substrates. Recent advances in this field includes the development of bulk-heterojunction devices, in which electron donor and electron acceptor species are mixed in solution, and subsequently spin cast onto a substrate [1–3]. As the solution evaporates, the two species form an interpenetrating network of domains [4]. When a photon is absorbed in either material an exciton excited state is formed. It has been shown that this exciton dissociates at interfaces between donor and acceptor species into a hole on the donor and an electron on the acceptor [5]. The separated charges are transported through their respective networks to the electrodes. In experiments with bi-layer photovoltaic devices it has been shown that the exciton diffusion length in typical materials is between 5 nm and 10 nm, and that only photons that are absorbed within the exciton diffusion length of a donor acceptor interface will separate into a charge pair [6]. This particular problem is overcome in the bulk heterojunction architecture because a well designed device has domains that are on the order of the exciton diffusion length, which yields near unity charge separation [7, 8].

In a series of recent articles, bulk heterojunction solar cells made from mixtures of [6,6]-phenyl C_{61}-butyric acid methyl ester (PCBM) and regio-regular poly(3-hexylthiophene) (P3HT) have reached power efficiencies of over 4% under AM1.5 illumination [9–11]. These devices show external quantum efficiencies (EQE) of up to 70% near the absorption maximum of the P3HT. In this article, we investigate whether the EQE could be improved, particularly in parts of the spectrum far from the absorption peak. From the published data, it is not clear whether the excess light is being reflected, absorbed in the indium tin oxide (ITO) layer, absorbed in the poly(3,4-ethylenedioxythiophene):poly(styrene sulfonic acid) (PEDOT:PSS) layer, or if the light is absorbed in the active layer and the EQE is lowered due to recombination effects.

Pettersson et al. produced an optical model [12] of bi-layer organic solar cells that can be used to model the photocurrent action spectra. This model is based upon the Fresnel relations for reflection and transmission and employs a matrix method for the calculation of optical intensity in multiple layer devices. This model is very successful for the design of bi-layer devices and has also been used to calculate the optimal layer thicknesses for vapor deposited tandem solar cells [13, 14]. Furthermore, the matrix model allows the calculation of optical intensity as a function of depth within the active layer of a photovoltaic device. The Petterson model does not, however, quantify the optical power dissipation in the various layers nor has it been used to make predictions of the EQE or internal quantum efficiency (IQE). A more recent optical model of bulk heterojunction solar cells from Hoppe et al. extended the Pettersson model to include estimates of the internal quantum efficiency (IQE) and current density as a function of active layer thickness for AM1.5 illumination [15] in MDMO-PPV:PCBM devices. Our own group has recently published an article that compares measured EQE in P3HT:PCBM devices with modeled optical intensity distributions as a function of active layer thickness [16].

In this study, an optical model of P3HT:PCBM bulk heterojunction solar cells is presented that quantifies the optical losses in completed devices, makes predictions for the

✉ Fax: +49-221-470-5144, E-mail: klaus.meerholz@uni-koeln.de

maximum possible EQE (EQEmax), and from this model calculates the maximum possible short current density (J_{sc}max) as a function of active layer thickness. Once a method for the calculation of J_{sc}max is established, a solar cell can be optimized by varying the layer thicknesses of the ITO, PEDOT:PSS, and active layer to maximize the dissipation of solar radiation in the active layer. Also considered is the exchange of materials to improve the optical properties of the solar cell. Finally, because of the recent interest in low band gap polymer solar cells, a model low band gap spectrum is analyzed to show the necessity in minimizing optical losses.

2 Optical modelling

The model described in this article concerns the dissipation of incident light into the various thin film layers of a polymer solar cell. It is assumed here that the device is fabricated by spin coating various polymer layers onto a commercially produced glass-ITO substrate, followed by deposition of a metal layer by evaporation (Fig. 1). The layers are considered to be parallel, smooth and of uniform thickness.

It is assumed that a collimated photon source is directed at a given sample with irradiance (I_0)

$$I_0 = \frac{c\varepsilon_0 \left(E_0^+\right)^2}{2}\,, \tag{1}$$

where c is the speed of light, ε_0 is the permittivity of free space, and E_0^+ is the amplitude of the incident electric field. When the photons meet the sample surface they can either be reflected or transmitted into the layers. The reflection and transmission at the air–glass interface is treated separate to the rest of the layer stack because the glass itself is optically "thick" and does not contribute to interference within the active layer of the solar cell. The reduction in E_0^+ and therefore I_0 is calculated using the Fresnel relation for transmission whereby,

$$E_1^+ = E_0^+ \left(\frac{2n_1}{n_0 + n_1}\right) \tag{2}$$

for radiation normal to the surface. This corresponds to the expected $\sim 4\%$ loss of irradiance intensity for an air–glass interface. This loss can be reduced by applying various antireflective coatings to the glass surface [17].

A simple method for the mathematical treatment for optical interference in multiple-layer thin-film stacks has been long established [17]. This method relies on a description of optically homogeneous layers aligned parallel to each other.

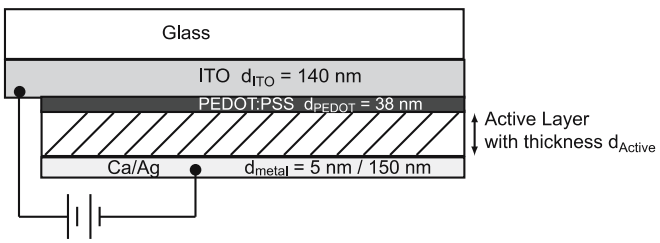

FIGURE 1 Schematic diagram of the standard bulk heterojunction solar cell used in this publication

In this case the optical properties, of both the materials and the interfaces, can be represented by 2×2 matrices due to the fact that the equations governing the propagation of the electric field are linear and that the tangential component of the electric field is continuous. The propagation of an incident electric field $\left(E_0^+\right)$ through layers $1{-}g$ is described by a propagation matrix S(i,j), where the indices i and j indicate the position within the matrix. All of the transmission, reflection, phase change, and absorption information for the entire stack are contained in the propagation matrix, including multiple reflections. Beginning from the forward radiation within the glass,

$$\begin{bmatrix} E_1^+ \\ E_1^- \end{bmatrix} = S \begin{bmatrix} E_{g+1}^+ \\ E_{g+1}^- \end{bmatrix}, \tag{3}$$

where E_1^+ is the electric field amplitude incident from the glass substrate, E_1^- is the reflected electric field amplitude, E_{g+1}^+ is the transmitted electric field amplitude and E_{g+1}^- is zero because no light originates from behind the metal electrode. The propagation matrix is

$$S = I_{12}\, L_2\, I_{23}\, \ldots\, I_{fg}\, L_g\, I_{g(g+1)}\,, \tag{4}$$

where I_{fg} and L_g are the 2×2 matrices describing the interface transmission–reflection and layer phase change-absorption of the various layers, respectively. In the case of an optically thick metal back electrode, no light is transmitted through the entire device. Dissipation within the metal (D_{metal}), reflection from the sample (R_{Total}) and dissipation within all of the other layers (D_{total}), can be measured as the fraction of incident illumination through the entire stack. These terms are calculated as

$$D_{metal} = \frac{n_{metal}}{n_{glass}} \left|\frac{E_1}{S(1,1)}\right|^2\,, \tag{5}$$

$$R_{Total} = \left|E_1 \frac{S(2,1)}{S(1,1)}\right|^2\,, \text{ and} \tag{6}$$

$$D_{total} = 1 - (D_{metal} + R_{Total})\,. \tag{7}$$

We assume in this case that the sum total of the incident illumination can be described by

$$R + D_{metal} + \sum_g D_g = 1\,. \tag{8}$$

The time average of the energy dissipated per second in a layer g as a function of distance from the front junction is described as

$$Q_g(x) = \frac{2\pi c\varepsilon_0 k_g n_g \left|E_g(x)\right|^2}{\lambda} \tag{9}$$

where $\left|E_g(x)\right|^2$ is the squared modulus of the electric field [12]. It has already been shown that integration over $Q_g(x)$ gives a measurement of the total energy dissipation in the active layer [16]. The dissipation of light in the ITO (D_{ITO}), PEDOT:PSS (D_{PEDOT}), and active layers (D_{Active}) can

be separated by calculating the distributions and then integrating across the layer for total energy dissipation within the layer, followed by normalizing to D_{total}.

$$D_{\text{ITO}} = D_{\text{total}} \frac{\int_0^{L_{\text{ITO}}} Q_{\text{ITO}}(x)\,\mathrm{d}x}{\sum_g \int_0^{L_g} Q_g(x)\,\mathrm{d}x}, \text{ etc. for all layers.} \quad (10)$$

One of the most indicative quantities calculated in the description of solar cells is the external quantum efficiency (EQE). This is a measurement of the ratio of electrons collected at the electrodes to photons incident on the device surface. EQE is typically calculated as

$$\text{EQE} = \frac{hcJ_{\text{sc}}}{I_0 \lambda q} 100, \quad (11)$$

where q is the electron charge and J_{sc} is the short circuit current density. Using the optical model presented above, another measure of the quantum efficiency is derived. The maximum possible EQE (EQEmax) for a given excitation wavelength is equivalent to the fraction of the energy dissipated in the active layer

$$\text{EQEmax} = D_{\text{Active}}\, 100, \quad (12)$$

for a given excitation wavelength over the band gap, and represents the loss free EQE. EQEmax is the EQE assuming that every photon dissipated in the active layer contributes to the measured current.

3 Experimental

3.1 *Sample preparation*

All of the solar cells in this work were prepared on commercial Indium-Tin Oxide (ITO) coated glass with layer thickness $\sim$ 140 nm and 15 Ω sheet resistance (Merck). The ITO is etched with acid and subsequently cleaned using chloroform, acetone, Mucasol detergent, and de-ionized water in an ultra-sonic bath. The cleaned ITO samples were exposed to ozone for 10 min and immediately spin coated with 38 nm of poly(3-4 ethylenedioxythiophene)polystyrene sulfonate (PEDOT:PSS) (Baytron P AL 4083, HC Stark). The PEDOT:PSS coated samples were heat treated at 110 °C for 3 min and then moved to a N_2 glovebox for the remainder of the fabrication and measurement. All polymer solutions were stirred overnight at 60 °C before spin coating to ensure that the polymer has been completely dissolved. The active layer of the solar cells are spin coated from a 1 : 1 mixture of regio-regular poly(3-hexylthiophene) (P3HT) (Aldrich, reported regio-regularity of > 98.5%) and [6,6]-phenyl C_{61}-butyric acid methyl ester (PCBM) (nano-C). The P3HT was cleaned twice prior to making the final solution by dissolving the polymer into chlorobenzene and crashing the solution into a 7 : 1 methanol-water solution, followed by filtration and drying under vacuum. All solar cells are spin coated from a chlorobenzene solution. Thickness variation was achieved through variation of the solution concentration and spinning speed. After spin coating the active layer, the samples were moved to a high vacuum chamber ($\sim 10^{-6}$ mbar), where an electrode of 5 nm Ca and 150 nm Ag was vapor deposited through a mask leaving seven solar cells with an active area of 7.85 mm^2. After metal deposition, the samples were tempered for 15 min at 140 °C in a N_2 atmosphere.

3.2 *Measurements*

The I–V curves of the samples were measured using a Keithley 2425 source measurement unit in an N_2 glovebox. The AM1.5 solar simulation light source (100 mW/cm^2) was provided by a filtered Xe lamp (150 W Oriel). The light intensity was calibrated using a calibrated solar cell from the Frauenhofer Institute for solar cell research (ISE) in Freiburg, Germany. Measurements of the complex refractive index (N) were performed using spectroscopic ellipsometry for the metal, ITO and PEDOT:PSS layers (nanofilm). The N for the active layer was measured using a partial reflection fitting technique because accurate optical constants could not be obtained using ellipsometry (publication in preparation). Sample thickness was determined using a Dektak surface profiler that was calibrated to a $\text{Si}-\text{SiO}_2$ ellipsometry standard.

4 Results and discussion

4.1 *Dissipation of incident illumination*

In order to optimize the performance of a solar cell it is necessary to quantify the sources of optical losses within the device. As has already been stated, a loss of $\sim$ 4% occurs due to reflection at the air–glass interface. The other sources of loss are plotted in Fig. 2 as functions of active layer thickness (d_{Active}). The greatest source of loss is due to reflection out of the device (R) (Fig. 2a). Incident radiation is reflected off of each of the interfaces glass-ITO, ITO-PEDOT:PSS etc. Reflection here considers all of the light coming back from the device after multiple reflections within the layer stack. For the typical 100 nm solar cell, optical losses from reflection total $\sim$ 30% of the incident radiation over the absorption band of the P3HT:PCBM device. This reflection means that the EQE of a 100 nm solar cell is absorption limited. The other sources of optical loss, dissipation in the metal (D_{metal}) (Fig. 2b), dissipation in the PEDOT:PSS layer (D_{PEDOT}) (Fig. 2c), and dissipation in the ITO layer (D_{ITO}) (Fig. 2d) also contribute to the reduced performance of the solar cells. The second highest loss is dissipation in the Al metal electrode. Since Ag is more reflective than Al, a 5 nm Ca/100 nm Ag electrode absorbs less light at all wavelengths than an Al electrode. The optical properties of Ca could not be measured with our ellipsometer because it oxidizes quickly in air so the values were taken from the literature [18]. The metal dissipation can be reduced by 3% if a Ca/Ag electrode is used instead of Al. Optical losses could also be reduced if the PEDOT:PSS and ITO could be made less absorbing at 400 nm. The EQEmax could be improved by 10%–15% at this wavelength through electrode exchange. It is clear that a systematic approach to loss reduction can yield improved solar cell performance.

Using the same methodology, the fraction of incident radiation dissipated in the active layer can also be calculated. As

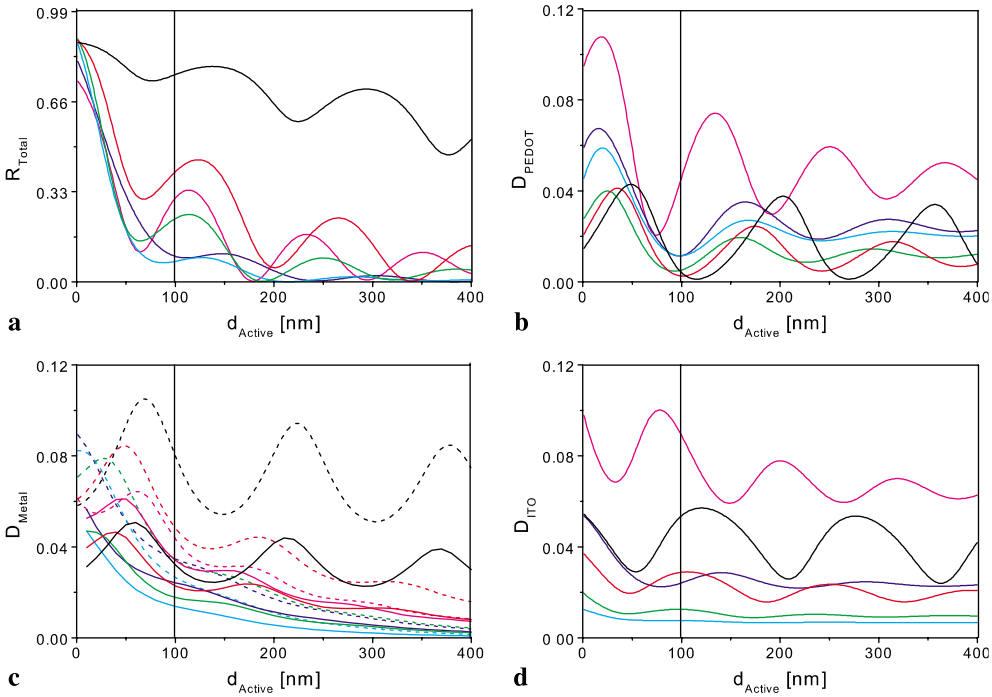

FIGURE 2 Fraction of the incident light energy that is reflected from the device (**a**), dissipated in the PEDOT:PSS layer (**b**), dissipated in the metal electrode (**c**), and dissipated in the ITO layer (**d**) as a function of active layer thickness for the illumination wavelengths 400 nm (*magenta*), 450 nm (*blue*), 500 nm (*cyan*), 550 nm (*green*), 600 nm (*red*), and 650 nm (*black*). In the plot for D_{metal}, dissipation for a Ca/Ag electrode is depicted as *solid lines* and an Al electrode is depicted by *dashed lines*. $d_{\text{ITO}} = 140$ nm and $d_{\text{PEDOT}} = 40$ nm are assumed for all calculations. The *horizontal black line* in each plot depicts a 100 nm active layer

shown in e.g. 12, if the assumption is made that all absorbed photons contribute one electron to the measured current, the EQEmax can be calculated (Fig. 3). Of interest in this figure is the large variations in the EQEmax with increased active layer thickness. Optical interference between the mirror like back electrode and the various interfaces creates a very uneven distribution of light and a periodic variance of light in the active layer.

Another question that can be answered with this optical model is: what is the optically limited efficiency of the solar cell under white light conditions? In order to answer this question, the EQEmax is calculated for optically thick devices across the absorption spectrum. Depicted in Fig. 3 are the calculated EQEmax vs. d_{Active} for wavelengths for optically thick devices ($d_{\text{Active}} = 5$–7 μm). It can be seen that the EQEmax's of between 80% and 94% are achieved across the entire spectrum. Considering that ∼ 4% of the total light is lost to reflection off the front glass, it is clear that schemes to increase light coupling to the active layer such as roughening or nano-structuring the various interfaces are more labor intensive that the expected gain is worth.

4.2 *Calculation and optimization of* J_{sc}max

The EQEmax(λ) can be summed and scaled for the AM1.5 illumination intensity to calculate J_{sc}max, which is a calculation of the J_{sc} with the assumption that all photons absorbed contribute to the measured current. In Fig. 4, the measured J_{sc} (stars) and calculated J_{sc}max (solid line) are plotted as a function of active layer thickness. It can be

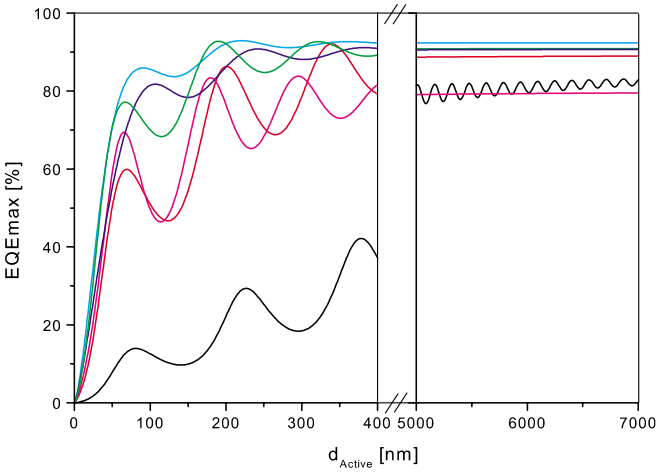

FIGURE 3 EQEmax vs. d_{Active} for 400 nm (*magenta*), 450 nm (*blue*), 500 nm (*cyan*), 550 nm (*green*), 600 nm (*red*) and 650 nm (*black*) illumination. $d_{\text{ITO}} = 140$ nm and $d_{\text{PEDOT}} = 40$ nm is assumed for all calculations

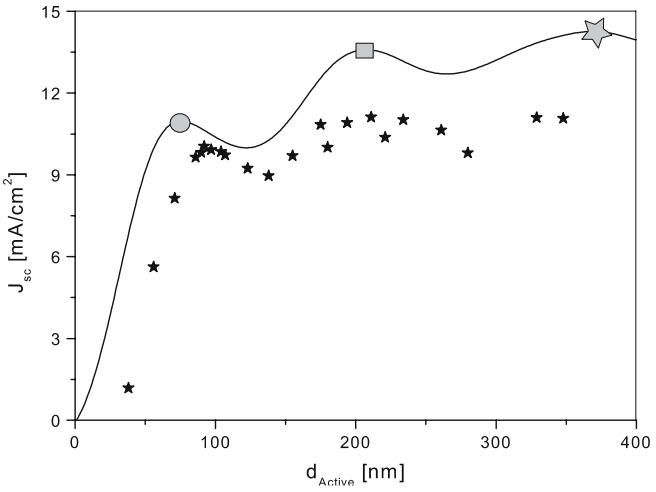

FIGURE 4 Depicted are the measured J_{sc} (*stars*) and the calculated J_{sc}max (*solid line*). The large *grey shapes* represent the maxima in J_{sc}max with standard d_{ITO}, and d_{PEDOT} that are further optimised in Fig. 5

clearly seen that both the measured and calculated data show light-dissipation-induced periodic modulation of the current as a function of active layer thickness. Furthermore, due to the high quality of the P3HT:PCBM solar cells, three peaks in the J_{sc} can clearly be discerned with the thickest active layers showing the highest current. We find that the I–V characteristics are nearly identical with those published by Li et al. [10] and due to reduced filling factor with increased active layer thickness, we achieve high efficiencies of between 4.3% and 4.4% for each peak in the measured J_{sc}. Since the optical losses have already been removed in the calculation of J_{sc}max, the difference between the measured J_{sc} and J_{sc}max is due to recombination in the active layer of the device [19–21].

Since the filling factor and open circuit voltage of a P3HT:PCBM solar cell has already been optimised [9, 10], it stands to reason that the only way to further optimize the device is to improve the optical input to the active layer. Simultaneous analysis of the J_{sc}max as functions of d_{ITO}, d_{PEDOT}, and d_{Acitve} can be performed. In this calculation a three dimensional matrix of data is generated with each of the three layer thicknesses as axis and J_{sc}max as the matrix values. Displayed in Fig. 5 are slices through this 3d data set for active layer thicknesses marked by the grey circle, square and triangle in Fig. 4 with $d_{Active} = 80$ nm, 220 nm, and 370 nm, respectively. The d_{ITO} and d_{PEDOT} values used for the measured data in this work are depicted as grey points on the figure. It is clear that reducing d_{PEDOT}, or replacing this layer with an electrode material that absorbs less light would lead directly to improved device efficiency. For both, the 80 nm and 220 nm data, an interplay exists between the optimal d_{ITO} and d_{PEDOT}, i.e. both must be changed simultaneously to gain the maximum improvement. Optimization of both layer thicknesses yields an improvement in J_{sc}max of between 0.6–0.8 mA/cm^2. These calculations consider the optical properties of the solar cell and not the electrical necessities of low sheet resistance or the prevention of pin hole formation. Nevertheless, this represents a potential improvement of ∼5%–9% when only changing the electrode layer thicknesses.

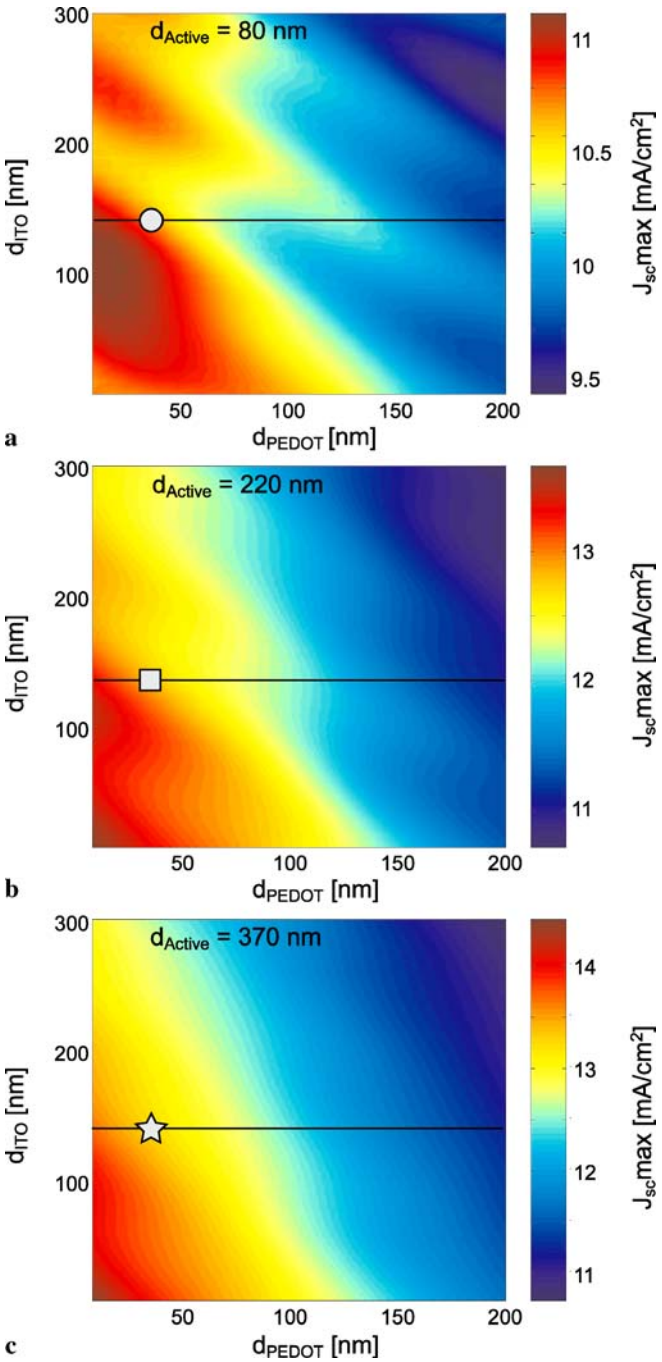

FIGURE 5 J_{sc}max as functions of d_{ITO} and d_{PEDOT} for d_{Active} of 80 nm (**a**), 220 nm (**b**) and 370 nm (**c**). *Grey marks* show the relative location of the measured values for $d_{ITO} = 140$ nm and $d_{PEDOT} = 38$ nm. The *black line* shows the potential J_{sc}max change for a constant d_{ITO} thickness

4.3 *Optimization of a model low band gap polymer*

The ITO substrates commercially available and typically used for polymer solar cell research are identical to those used for flat screen monitors and televisions and, therefore, are optimised for the transmission of ∼ 500 nm light, which is ideal for the spectrum visible to the human eye. In an effort to improve the absorption range of polymer solar cells, a number of research groups are developing low band gap polymers [22, 23] and nanoparticle polymer mixtures [24, 25]. The absorption maximum of these materials is between 600 nm and 900 nm, which means that the standard ITO thickness is non-ideal. The EQE's of the solar cells made from these new low band gap devices are typically less than 30%. In order to determine whether the low EQE values are in part due to high optical losses, we model two Lorentzian low band gap spectra centered at 750 nm (Fig. 6a) with low and high extinction coefficient (κ), respectively. The high κ spectrum has a maximum of $\kappa = 0.39$, which is identical to the maximum of the P3HT:PCBM absorption band. $\kappa = 0.0925$ is assumed for the maximum of the low absorption spectrum and is probably more representative of the typical low band gap absorber. For direct comparison, high band gap Lorentzian spectra, centered at 500 nm, with the same κ distribution, and covering the same band width on the energy scale, are also modelled. All model calculations are made with the assumption of $n = 1.8$.

When the J_{sc}max for an inorganic semiconductor solar cell is calculated, all of the photons with energy higher than the band gap can contribute to the measured current. For

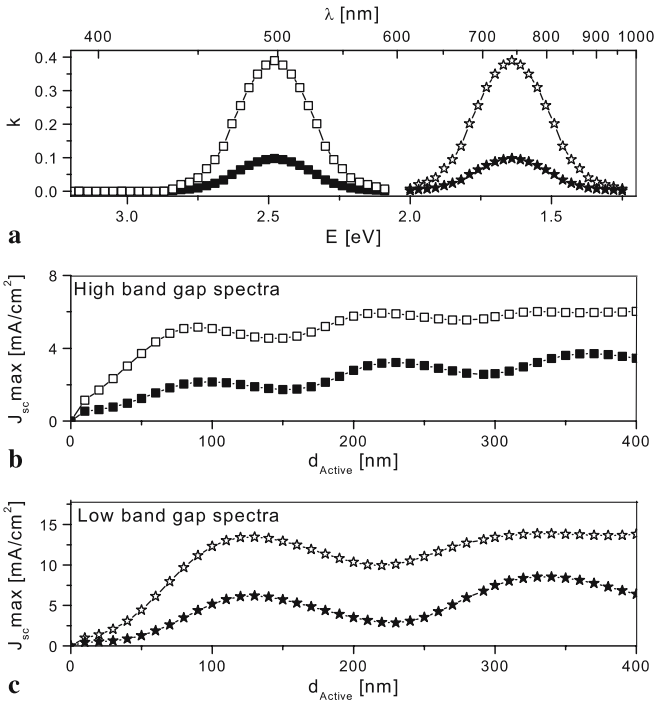

FIGURE 6 Model Lorentzian high (*squares*) and low (*stars*) band gap spectra centered at 500 nm and 750 nm, respectively. For comparison, low (*filled*) and high (*open*) extinction coefficients are included (**a**). Calculated J_{sc}max vs. d_{Active} for the sample spectra assuming the standard $d_{ITO} = 140$ nm and $d_{PEDOT} = 38$ nm for the high (**b**) and low (**c**) band gap spectra

a polymer or Lorentzian spectrum, only photons within the absorption spectrum of the polymer can contribute to the current, which means that the spectrum is bound by both a minimum and a maximum. J_{sc}max of 21.2 mA/cm^2 and 8.6 mA/cm^2 for the low and high band gap spectra, respectively, can be calculated assuming 100% EQE over the entire band. Due to the difference in photon densities in the AM1.5 spectrum, the low band gap spectrum has a much higher J_{sc}max. The EQEmax (not shown) of the high band gap spectra can reach $\sim$ 90% and the low band gap spectrum peaks at $\sim$ 82% for optically thick samples. This result shows that the optically limited EQE of the low band gap polymers is only 8% lower than the high band gap polymers due to the non-ideal clear electrode thicknesses.

Examination of the J_{sc}max data in Fig. 6b and Fig. 6c, show that the interference induced maxima are shifted to longer wavelengths for the low band gap polymer from $\sim$ 80 nm and $\sim$ 220 nm to $\sim$ 130 nm and $\sim$ 330 nm. The first maximum in J_{sc}max for the low band gap spectrum is found for the same d_{Active} as the first minimum for the high band gap spectrum. This shows that it is not possible to optimize the active layer thickness for both high and low band gap conditions simultaneously. The J_{sc}max for the high κ spectra quickly approaches the absorption limit with the first thickness maximum showing over 60% of the photons within the band absorbed. Given that the measured EQE of the reported low band gap polymer solar cells [23] lies in the range of 20%, it is likely that low absorption limits the performance of these devices. In this case, the greatest optical loss mechanism is reflection and the way to increase the performance of these devices is to increase d_{Active}.

5 Summary and conclusions

We have utilized an optical model for polymer/fullerene solar cells that allows for quantitative analysis of light dissipation in the various layers of a complete solar cell device. The model calculates the maximum possible EQE by subtracting the optical losses from all of the layer materials including the substrate. Examination of the individual losses as a function of wavelength allows systematic analysis of the materials used for electrode materials. Integration over the EQEmax and AM1.5 spectrum at an intensity of 100 mW/cm^2 allows the calculation of the light dissipation limited J_{sc}. Examination of this J_{sc}max indicates a strong periodic variation in the quantity of light dissipated in the active layer of a solar cell as a function of active layer thickness, and measurement of the J_{sc} in P3HT:PCBM based solar cells confirms this prediction. Optimization of the clear electrode layer thicknesses, metal electrode reflection and active layer thickness all yield quantifiable improvements in the J_{sc}max, particularly for absorption of solar radiation far from the absorption maximum of the active layer.

A comparison between model Lorentzian low and high band gap spectra was made to show the effect of the band gap on the optimum active layer thicknesses. It was shown that the EQEmax for low band gap materials is not limited by optical losses in the transparent electrodes. Low EQE seen in devices reported in the literature are therefore, due either to low internal efficiency or to low absorption. Our recommendation is that devices with a larger active layer thickness be fabricated.

ACKNOWLEDGEMENTS We would like to acknowledge the Alexander von Humboldt foundation for the post doctoral grant to A.Moule. We would also like to thank the German Ministry of Science and Education (BMBF) for funding the EKOS project (O3N2023D), and Prof. John Logan (San Jose St. Univ.) for programming advice.

REFERENCES

1 J.J.M. Halls, C.A. Walsh, N.C. Greenham, E.A. Marseglia, R.H. Friend, S.C. Moratti, A.B. Holmes, Nature **376**, 498 (1995)
2 K.M. Coakley, M.D. McGehee, Chem. Mater. **16**, 4533 (2004)
3 G. Yu, J. Gao, J.C. Hummelen, F. Wudl, A.J. Heeger, Science **270**, 1789 (1995)
4 H. Hoppe, M. Niggemann, C. Winder, J. Kraut, R. Hiesgen, A. Hinsch, D. Meissner, N.S. Sariciftci, Adv. Funct. Mater. **14**, 1005 (2004)
5 N.S. Sariciftci, L. Smilowitz, A.J. Heeger, F. Wudl, Science **258**, 1474 (1992)
6 D.E. Markov, E. Amsterdam, P.W.M. Blom, A.B. Sieval, J.C. Hummelen, J. Phys. Chem. A **109**, 5266 (2005)
7 S.E. Shaheen, C.J. Brabec, N.S. Sariciftci, F. Padinger, T. Fromherz, J.C. Hummelen, Appl. Phys. Lett. **78**, 841 (2001)
8 J.K.J. van Duren, X.N. Yang, J. Loos, C.W.T. Bulle-Lieuwma, A.B. Sieval, J.C. Hummelen, R.A.J. Janssen, Adv. Funct. Mater. **14**, 425 (2004)
9 W. Ma, C. Yang, X. Gong, K. Lee, A.J. Heeger, Adv. Funct. Mater. **15**, 1617 (2005)
10 G. Li, V. Shrotriya, J. Huang, Y. Yao, T. Moriarty, K. Emery, Y. Yang, Nature Mater. **4**, 864 (2005)
11 M. Reyes-Reyes, K. Kim, D.L. Carroll, Appl. Phys. Lett. **87**, 083 506 (2005)
12 L.A.A. Pettersson, L.S. Roman, O. Inganas, J. Appl. Phys. **86**, 487 (1999)
13 J.G. Xue, S. Uchida, B.P. Rand, S.R. Forrest, Appl. Phys. Lett. **85**, 5757 (2004)
14 J. Drechsel, B. Mannig, F. Kozlowski, M. Pfeiffer, K. Leo, H. Hoppe, Appl. Phys. Lett. **86**, 244 102 (2005)
15 H. Hoppe, N. Arnold, N.S. Sariciftci, D. Meissner, Sol. Ener. Mater. Solar Cells **80**, 105 (2003)

16 A.J. Moulé, J.B. Bonekamp, K. Meerholz, J. Appl. Phys. **100**, 094 503 (2006)
17 E. Hecht, *Optics*, 4th. ed. (Pearson, San Francisco, 2002)
18 C.M. Ramsdale, N.C. Greenham, J. Phys. D Appl. Phys. **36**, L29 (2003)
19 L.J.A. Koster, V.D. Mihailetchi, P.W.M. Blom, Appl. Phys. Lett. **88**, 052 104 (2006)
20 L.J.A. Koster, E.C.P. Smits, V.D. Mihailetchi, P.W.M. Blom, Phys. Rev. B **72**, 085 205 (2005)
21 A.J. Moule, K. Meerholz, submitted to Appl. Phys. Lett. (2006)
22 B.P. Rand, J.G. Xue, F. Yang, S.R. Forrest, Appl. Phys. Lett. **87**, 200 508 (2005)
23 M.M. Wienk, M.G.R. Turbiez, M.P. Struijk, M. Fonrodona, R.A.J. Janssen, Appl. Phys. Lett. **88**, 153 511 (2006)
24 S. Zhang, P.W. Cyr, S.A. McDonald, G. Konstantatos, E.H. Sargent, Appl. Phys. Lett. **87**, 233 101 (2005)
25 E. Arici, H. Hoppe, F. Schaffler, D. Meissner, M.A. Malik, N.S. Sariciftci, Appl. Phys. A **79**, 59 (2004)